



GMP-Compliant Extracellular Vesicles Derived From Umbilical Cord Mesenchymal Stromal Cells: Manufacturing and Preclinical Evaluation in ARDS treatment

Zaquer Suzana Munhoz Costa Ferro , Gisele Vieira Rocha ,
Katia Nunes da Silva , Bruno Diaz Paredes , Erick Correia Loiola ,
Johnatas Dutra Silva , John Lenon de Souza Santos ,
Rosane Borges Dias , Cláudio Pereira Figueira ,
Camila Indiani de Oliveira , Ludmilla David de Moura ,
Lígia Nunes de Moraes Ribeiro , Eneida de Paula ,
Dalila Lucíola Zanette , Clarissa Araújo Gurgel Rocha ,
Patricia Rieken Macedo Rocco , Bruno Solano de Freitas Souza

PII: S1465-3249(24)00686-8
DOI: <https://doi.org/10.1016/j.jcyt.2024.04.074>
Reference: JCYT 1768

To appear in: *Cytotherapy*

Received date: 14 February 2024
Accepted date: 27 April 2024

Please cite this article as: Zaquer Suzana Munhoz Costa Ferro , Gisele Vieira Rocha ,
Katia Nunes da Silva , Bruno Diaz Paredes , Erick Correia Loiola , Johnatas Dutra Silva ,
John Lenon de Souza Santos , Rosane Borges Dias , Cláudio Pereira Figueira ,
Camila Indiani de Oliveira , Ludmilla David de Moura , Lígia Nunes de Moraes Ribeiro ,
Eneida de Paula , Dalila Lucíola Zanette , Clarissa Araújo Gurgel Rocha , Patricia Rieken Macedo Rocco ,
Bruno Solano de Freitas Souza , GMP-Compliant Extracellular Vesicles Derived From Umbilical Cord
Mesenchymal Stromal Cells: Manufacturing and Preclinical Evaluation in ARDS treatment, *Cytother-*
apy (2024), doi: <https://doi.org/10.1016/j.jcyt.2024.04.074>

This is a PDF file of an article that has undergone enhancements after acceptance, such as the addition of a cover page and metadata, and formatting for readability, but it is not yet the definitive version of record. This version will undergo additional copyediting, typesetting and review before it is published in its final form, but we are providing this version to give early visibility of the article. Please note that, during the production process, errors may be discovered which could affect the content, and all legal disclaimers that apply to the journal pertain.

GMP-Compliant Extracellular Vesicles Derived From Umbilical Cord Mesenchymal Stromal Cells: Manufacturing and Preclinical Evaluation in ARDS treatment

Zaquer Suzana Munhoz Costa Ferro^{1,2}, Gisele Vieira Rocha^{1,2}, Katia Nunes da Silva¹, Bruno Diaz Paredes^{1,2}, Erick Correia Loiola^{1,2}, Johnatas Dutra Silva⁸⁻¹⁰, John Lenon de Souza Santos^{1,3}, Rosane Borges Dias^{3,4}, Cláudio Pereira Figueira³, Camila Indiani de Oliveira³, Ludmilla David de Moura⁶, Lígia Nunes de Moraes Ribeiro^{6,7}, Eneida de Paula⁶, Dalila Lucíola Zanette⁵, Clarissa Araújo Gurgel Rocha¹⁻⁴, Patricia Rieken Macedo Rocco⁸⁻¹⁰, Bruno Solano de Freitas Souza^{1-3*}

¹Center for Biotechnology and Cell Therapy, São Rafael Hospital, Salvador, Brazil

²D'Or Institute for Research and Education (IDOR), Salvador, Brazil

³Gonçalo Moniz Institute, FIOCRUZ, Salvador, Brazil

⁴Federal University of Bahia, UFBA, Salvador, Brazil

⁵Carlos Chagas Institute, FIOCRUZ, Curitiba, Brazil

⁶Institute of Biology, University of Campinas, Campinas, São Paulo, Brazil

⁷Institute of Biotechnology, Federal University of Uberlândia, Uberlândia, Brazil

⁸Laboratory of Pulmonary Investigation, Carlos Chagas Filho Institute of Biophysics, Federal University of Rio de Janeiro, Rio de Janeiro, Brazil

⁹National Institute of Science and Technology for Regenerative Medicine, Rio de Janeiro, Brazil

¹⁰Rio de Janeiro Innovation Network in Nanosystems for Health-NanoSaúde, Research Support Foundation of the State of Rio de Janeiro, Rio de Janeiro, Brazil.

*Correspondence: Bruno S.F. Souza, MD, PhD, Instituto Gonçalo Moniz, Fundação Oswaldo Cruz, Rua Waldemar Falcão, 121, Salvador, Brasil. CEP: 40296-710. Tel: +557131762260. E-mail address: bruno.solano@fiocruz.br

Abstract

Background aims: Extracellular vesicles (EVs) represent a new axis of intercellular communication that can be harnessed for therapeutic purposes, as cell-free therapies. The clinical application of mesenchymal stromal cell (MSC)-derived EVs, however, is still in its infancy and faces many challenges. The heterogeneity inherent to MSCs, differences among donors, tissue sources, and variations in manufacturing conditions may influence the release of EVs and their cargo, thus potentially affecting the quality and consistency of the final product. We investigated the influence of cell culture and conditioned medium harvesting conditions on the physicochemical and proteomic profile of human umbilical cord MSC-derived EVs (hUCMSC-EVs) produced under current good manufacturing practice (cGMP) standards. We also evaluated the efficiency of the protocol in terms of yield, purity, productivity, and expression of surface markers, and assessed the biodistribution, toxicity and potential efficacy of hUCMSC-EVs in preclinical studies using the LPS-induced acute lung injury model. **Methods:** hUCMSCs were isolated from a cord tissue, cultured, cryopreserved, and characterized at a cGMP facility. The conditioned medium was harvested at 24, 48, and 72 h after the addition of EV collection medium. Three conventional methods (nanoparticle tracking analysis, transmission electron microscopy, and nanoflow cytometry) and mass spectrometry were used to characterize hUCMSC-EVs. Safety (toxicity of single and repeated doses) and biodistribution were evaluated in naive mice after intravenous administration of the product. Efficacy was evaluated in an LPS-induced acute lung injury model. **Results:** hUCMSC-EVs were successfully isolated using a cGMP-compliant protocol. Comparison of hUCMSC-EVs purified from multiple harvests revealed progressive EV productivity and slight changes in the proteomic profile, presenting higher homogeneity at later timepoints of conditioned medium harvesting. Pooled hUCMSC-EVs showed a non-toxic profile after single and repeated intravenous administration to naive mice. Biodistribution studies demonstrated a major concentration in liver, spleen and lungs. HUCMSC-EVs reduced lung damage and inflammation in a model of LPS-induced acute lung injury. **Conclusion:** hUCMSC-EVs were successfully obtained following a cGMP-compliant protocol, with consistent characteristics and preclinical safety profile, supporting their future clinical development as cell-free therapies.

Keywords: mesenchymal stromal cells; extracellular vesicles; proteomics; preclinical; biodistribution; toxicity; ARDS.

Introduction

The therapeutic potential of MSCs is related to a plethora of immunomodulatory, anti-inflammatory, and pro-repair effects that are partially mediated by their secretome [1, 2]. Among the components of the MSCs' secretome, extracellular vesicles (EVs) attracted substantial interest because their therapeutic properties closely resemble those of their source cells [3, 4]. EVs are defined as cell-derived lipid bilayer membrane-delimited, nano- to micro-sized particles that cannot replicate on their own [5]. They can be classified, based on their biogenesis, as exosomes, microvesicles, apoptotic bodies, among others [6]. EVs are increasingly recognized as crucial mediators of intercellular communication in both healthy and disease states. They transport a diverse array of bioactive molecules such as cytosolic and transmembrane proteins, lipids, lipoproteins, integrins, growth factors, enzymes, mRNA, and microRNA (miRNA) [7-10]. Studies on EVs have the potential to drive the discovery of biomarkers and the development of cell-free therapies. [11].

Compared to living cell therapy products, EVs provide several benefits including simpler storage requirements, easier handling, enhanced stability, and straightforward usage, all of which significantly ease their distribution and practical application in real-world settings [12]. However, the clinical application of MSC-derived EVs (MSC-EVs) is still in its infancy and faces many challenges [13]. As for any medicine, the translational path of such products requires a demonstration of its quality, in vivo biodistribution, safety, and efficacy [14, 15]. The large-scale production of MSC-EVs under current good manufacturing practice (cGMP) standards must be implemented and validated for each product. Therefore, many ongoing studies have attempted to standardize the methods of isolation, purification, and characterization of MSC-EVs [16].

Variability in manufacturing conditions, in addition to the inherent heterogeneity of MSCs, may quantitatively and qualitatively influence the release of EVs and their cargo, eventually leading to poor quality and consistency of the final EV product [17]. The similarity between the samples at

every multiple-conditioned medium (CM) harvest also needs to be evaluated. Therefore, a deeper understanding of the EV biology, cargo, and functions, along with a precise and accurate characterization of MSC-EV-based products and data regarding their systemic distribution and delivery, are necessary to boost the development of such products for any clinical indication [2, 18].

Within the spectrum of clinical disorders subject to research for cellular and acellular therapeutic interventions, acute lung injury (ALI) represents a critical area of unmet medical necessity, exhibiting a favorable prospect for therapeutic innovation and progress in the field [19]. Acute respiratory distress syndrome (ARDS) is a severe form of ALI characterized by severe pulmonary inflammation and lung permeability leading to alveolar edema, hypoxemia, and pulmonary damage [20]. Despite extensive research efforts, the mortality rate among critically ill patients continues to be high, reaching approximately 40% [21]. Here, we aimed to provide novel insights for future MSC-EV research and treatment selection directed to ARDS. Here, we investigated the influence of the culture and harvesting conditions on the EV proteomic profile, productivity, and the expression of surface markers, and evaluated the biodistribution, toxicity, and therapeutic potential in LPS-induced ALI model.

Materials and methods

Production of human umbilical cord mesenchymal stromal cell-extracellular vesicles

Human umbilical cord MSC-derived EVs (hUCMSCs) were isolated from a single donor's cord tissue at the cGMP facility of the Center for Biotechnology and Cell Therapy, São Rafael Hospital, Salvador, Brazil. The characterization of hUCMSCs was performed using flow cytometry, trilineage differentiation assays, sterility tests, and other pertinent quality control measures [22]. HUCMSCs (p3) were obtained from the master cell bank, thawed, plated in stacks at a density of 4,000 cells/cm² (HyperFlask, Corning, NY, USA) and cultured in cGMP xeno-free growth medium (RoosterNourish; RoosterBio, Frederick, MD, USA). The growth medium was

removed when 80% confluence was achieved. After washing with Dulbecco's phosphate-buffered saline (CTS-DPBS; Thermo Fisher Scientific, Waltham, MA, USA), the EV collection medium was added (Rooster EV Collect, RoosterBio). The medium was harvested at 24, 48, and 72 h after adding the hUCMSC-EV collection medium. Cell count and viability were evaluated in an automatized cell counter LUNA FX7 (Logos Biosystems). The EV-enriched secretome was purified following either a cGMP-compliant protocol (tangential flow filtration using 650 μm and 500 kDa cartridges; Repligen, Waltham, MA) or a research-grade purification protocol, which was utilized for the biodistribution studies (total exosome isolation reagent; Thermo Fisher Scientific). Full characterization of the product included *Mycoplasma*, sterility, endotoxin, viral testing, among others, as previously described [22].

Nanoparticle tracking analysis

HUCMSC-EV samples were diluted in phosphate-buffered saline (PBS) and analyzed in terms of the nanoparticle size (nm), span (cumulative polydispersity index) and nanoparticle concentration (particles/mL), in a NanoSight NS300 instrument (Malvern Instruments, Malvern, UK) equipped with a sample chamber and a green (532 nm) laser. Samples were manually introduced into the chamber through sterile syringes. Three videos of 30 s each were captured, wherein approximately 2,000 tracks were counted in each measurement, run at room temperature (22-24 °C), as described previously [23].

Transmission electron microscopy

The morphology of hUCMSC-EVs was evaluated by transmission electron microscopy (TEM). Ten microliters of each hUCMSC-EV sample were applied to a formvar carbon-coated grid and held for 5 min for adsorption. The grid was dried, 10 μL of aqueous 2% uranyl citrate was added, and the grid was then incubated for 1 min. The excess stain was removed by touching the edge to a sheet of paper filter and allowing the grid to air dry for 24 h. The samples were observed in a JEOL 1230 microscope (JEOL, Tokyo, Japan) at 80 kV.

Nanoflow cytometry

For immunophenotyping of hUCMSC-EVs, we used a Cytoflex S cytometer (Beckman Coulter, Brea, CA, USA) configured for nanoflow following the equipment manual. After initial noise discrimination and employing the standard setup for nanoparticle size (Gigamix beads; BioCytex, Marseille, France), we selected a sub-population for analysis, whose sizes ranged between 100 and 500 nm. HUCMSC-EVs were stained with CD63-PE (Beckman Coulter), CD81-PE (Invitrogen, Waltham, MA, USA), and CD90-APC (BD Biosciences, Franklin Lakes, NJ, USA). The samples were incubated with the antibodies for 30 min at room temperature and protected from light. Samples were diluted (1:2,000) with the appropriate buffer before acquisition. Experiments were conducted following MiFlowCyt-EV guidelines [24]. Data analysis was conducted using the CytExpert v.2.5 software (Beckman Coulter).

Protein quantification

The total protein concentration was measured according to the manufacturer's instructions, using the Qubit protein assay kit and Qubit 4 fluorometer (Thermo Fisher Scientific).

Proteomic analysis

Protein extraction was conducted by incubating samples in a buffer containing 4% sodium dodecyl sulfate (SDS), 0.1 M dithiothreitol (DTT), 0.1 M Tris-HCl (pH 7.5), and protease inhibitors. Ten micrograms of the protein lysate were loaded into the denaturing polyacrylamide gel (10% sodium dodecyl-sulfate polyacrylamide gel electrophoresis (SDS-PAGE) solution) and stained with Coomassie blue. Bands were cut from the gel and discolored using a solution of 25 mM ethanol and 50% ammonium bicarbonate (ABC). The gel pieces were dehydrated and dried in a SpeedVac, then reduced (10 mM DTT solution in 50 mM ABC) and alkylated (55 mM iodoacetamide in 50 mM ABC). The liquid portion was discarded, and the fragments were digested with trypsin (50 mmol in ABC buffer) for 20 min at 4 °C. The excess trypsin solution

was removed, and digestion buffer was added to the fragments and incubated overnight at 37 °C. The peptides were extracted twice with acetonitrile under agitation for 10 min at 25 °C. The resulting sample was concentrated in a SpeedVac to 10–20% of the original volume. Peptides were purified with StageTips-C18, dried, and placed in a SpeedVac system for 30 min without heating. The sample was diluted in an AD solution (0.1% formic acid, 5% dimethyl sulfoxide, and 5% acetonitrile), for prompt analysis in a gradient for over 60 min by liquid chromatography-tandem mass spectrometry (LC-MS/MS) in an Eksigent NanoLC 1D plus liquid chromatography equipment. The analytical columns measured 15 cm with an internal diameter of 75 µm, containing 3 µm diameter C18 particles (Dr. Maisch, Ammerbuch, Germany). Mass spectrometry was conducted in a hybrid mass spectrometer equipment (LTQ Orbitrap XL ETD; Thermo Scientific). The top 10 most intense ions were fragmented, with CID30 and 30-s dynamic deletion. The mass spectrometry proteomics data were deposited to the Proteome X change Consortium via the Proteomics Identification (PRIDE) partner repository [25] with the dataset identifier PXD038850.

Differentially expressed protein analysis

Proteomics statistics were conducted based on label-free quantification (LFQ) of protein abundance processed with the MaxQuant platform. Identified proteins showing a false discovery rate value of $\geq 1\%$ were filtered. The generated “proteinGroups.txt” table was imported into R (version 4.2) to search for differentially expressed proteins.

The R package differential enrichment analysis of proteomics (DEP) data was used to analyze the differentially expressed proteins at 24, 48, and 72 h. The contaminant and reverse proteins were removed. The remaining data were filtered for proteins that showed an LFQ of > 0 in at least one group. The resulting LFQ intensities were normalized and imputed using random draws from a Gaussian distribution centered around a minimal value ($P < 0.01$). Finally, differential

enrichment analysis was conducted in DEP, using the Limma function, selecting proteins with P -adjusted and \log_2 (fold change) values of < 0.01 and > 1 , respectively.

Protein–protein interaction network analysis

The Search Tool for the Retrieval of Interacting Genes/Proteins (STRING) database (<https://string-db.org/>) was used to screen protein–protein interaction (PPI) networks with an interaction score of ≥ 0.7 . Cytoscape software (version 11.5) was used to illustrate the network. The enrichment analysis Cytoscape plug-in was used to identify significant Gene Ontology (GO) biological processes (BPs) for each network.

Gene set enrichment analysis

GO and Kyoto Encyclopedia of Genes and Genomes pathway enrichment analyses were conducted using the Database for Annotation, Visualization, and Integrated Discovery (DAVID) (david.ncifcrf.gov). Significance was defined at a cutoff of $P < 0.01$.

Animals

All experimental animal procedures followed the ARRIVE guidelines, and protocols were reviewed and approved by the Committee for the Use and Care of Animals in Research (CEUA) at Gonçalo Moniz Institute (Fiocruz, Bahia) under protocol number ID 021-2021, and by the Ethics Committee of the Health Sciences Center (127/21) at the Federal University of Rio de Janeiro. We followed the principles of the Guide for the Care and Use of Laboratory Animals proposed by the National Institute of Health (NIH). BALB/c mice (6–8 weeks old, weight 20-25 g) were randomized into different groups for the subsequent studies. The mice were housed in a temperature-controlled environment (23 ± 2 °C) with free access to food and water ad libitum under a 12/12 h light/dark cycle.

In vivo biodistribution study

To evaluate the in vivo biodistribution of hUCMSC-EVs after systemic administration, we used the lipophilic dye 1,1-dioctadecyl-3,3,3,3-tetramethylindotricarbocyanine iodide (DiR; Invitrogen), which provides an infrared fluorescent signal. DiR-labeled EVs (DiR-hUCMSC-EVs) were intravenously administered into naive mice via the tail vein, followed by euthanasia for ex-vivo fluorescence imaging. hUCMSC-EVs were incubated with 1 mM DiR at room temperature for 30 min before the isolation of hUCMSC-EVs by ultracentrifugation at $100,000 \times g$ for 2 h. Subsequently, the pellet was resuspended in PBS, purified, and stored at $-80\text{ }^{\circ}\text{C}$. DiR-hUCMSC-EVs ($30\text{ }\mu\text{g protein}/100\text{ }\mu\text{L}/\text{mouse}$, $n = 5$) or PBS solutions (PBS served as the control, $100\text{ }\mu\text{L}/\text{mouse}$, $n = 5$) were injected into the mice through the tail vein. The mice were euthanized at 1 and 24 h after injection for the subsequent ex-vivo analysis of organs. Images were captured with excitation/emission filters at 710/770 nm, respectively. The fluorescence signals in the tissues were analyzed using the AMI HTX BLI system (Spectral Instruments Imaging, Tucson, AZ, USA).

In vivo toxicity study

We evaluated the toxicity of a single dose of hUCMSC-EVs ($30\text{ }\mu\text{g protein}/100\text{ }\mu\text{L}/\text{mouse}$, $n = 5$ per group) at 24 h and 14 days (single intravenous (IV) administration), or after repeated administrations over either 3 or 6 weeks, as follows: hUCMSC-EVs were administered three times a week, the first dose was intravenously (IV) injected through the tail vein, and the second and third doses were administered by the intraperitoneal (IP) route for 3 weeks. One final IP dose was administered after 3 and 6 weeks of dosing, and all the mice were euthanized 1 day after the last dose.

Control groups received Plasma-Lyte [control (CTRL), $n = 5$] under the same conditions. The health status of the animals, including the body weight, visual and behavioral signs of toxicity and mortality, was measured daily. For all groups, blood samples were collected through the

submandibular vein for further hemogram, and biochemical analyses to evaluate the renal and hepatic functions, as described previously [26]. For biochemical analysis, the serum was separated by centrifugation at $3,000 \times g$ for 5 min to measure the aspartate aminotransferase (AST), alanine aminotransferase (ALT), blood urea nitrogen (BUN), and creatinine (Cr) in a certified laboratory.

The mice were euthanized by cervical dislocation and samples from the lungs, liver, brain, heart, and kidneys were excised and fixed in 10% formaldehyde. Fragments from the spleen were collected for analyses of the immunophenotype of cell sub-populations by flow cytometry.

Immunophenotyping of spleen sub-populations

Mouse spleens were gently homogenized, and the homogenate was washed with PBS and centrifuged at $340 \times g$ for 10 min at 4 °C. The supernatant was discarded and the red blood cell lysing solution (BD Pharmlyse, BD Biosciences) was added to the pellet. The suspension was centrifuged at $340 \times g$ for 10 min at 4 °C, resuspended in PBS and incubated with antibodies for B lymphocytes (CD45+/CD19), T lymphocytes (CD45+/CD3+), and macrophages (CD45+/CD11b+/F4-80+) for 20 min at RT. The following antibodies were utilized: CD45-PE-Cy5, CD19-PE, CD3-FITC, CD11b-FITC, CD11c-PE-Cy7, and F4-80-PE (all from BD Biosciences). Data were acquired using a Fortessa cytometer (BD Biosciences). Data analysis was conducted using the FlowJo (v10) software (FlowJo LLC).

Tissue processing and histology analysis

Macroscopy was conducted by a pathologist, and gross changes (e.g., size, shape, texture, color, etc.) were registered. Tissues were processed using a graded alcohol series, cleaned in xylene, and embedded in paraffin wax. The tissue was cut into 5 μm thick slices and stained with hematoxylin and eosin. The slides were scanned in an Axio Imager Z2/VSLIDE (Zeiss, Oberkochen, Germany) using 10 \times and 20 \times objectives [27]. Histologic findings that were present exclusively in the hUCMSC-EV-treated groups were classified as treatment-specific.

ALI model

ALI was induced in male mice by intratracheal administration of *Escherichia coli* lipopolysaccharide (LPS) (serotype O55:B5, LPS-B5 Ultrapure: TLR4 agonist; InvivoGen, San Diego, CA, USA) at a dose of 2 mg·kg⁻¹ (ARDSp). In control (C) groups, sterile saline solution was administered intratracheally (50 µL, Cp) instead. On the following day, ALI mice were further randomized into subgroups to receive sterile PBS solution (100 µL) or hUCMSC-EVs, all administered via the jugular vein. The total amount of hUCMSC-EVs administered was 60 µg into 100 µL of PBS. Twenty-four hours after treatment administration, lungs were collected for analysis.

Lung histology

A laparotomy was promptly conducted, and heparin (1,000 IU) was administered into the vena cava. The trachea was clamped at end-expiration (PEEP = 2 cmH₂O), and the abdominal aorta and vena cava were incised, resulting in a substantial hemorrhage that led to the rapid demise of the animals. The left lung was subsequently excised, fixed in 4% buffered formaldehyde, and embedded in paraffin. Sections (4 µm thick) were then cut and stained with hematoxylin-eosin. Photomicrographs at magnifications of x100, x200, and x400 were captured from four non-overlapping fields of view per section using a light microscope (Olympus BX51, Olympus Latin America-Inc., Brazil) [28].

Diffuse alveolar damage (DAD) was assessed employing a weighted scoring system by a researcher blinded to the experimental protocol, as previously described [29]. In short, scores ranging from 0 to 4 were assigned to denote the severity of septal thickening, alveolar collapse, inflammatory infiltration, and hemorrhage, where 0 indicated no effect and 4 represented maximum severity. Scores were computed as the product of the severity and extent of each feature, within a range of 0 to 16. The cumulative DAD score was then calculated as the sum of the scores for each characteristic, ranging from 0 to 64.

Enzyme-Linked Immunosorbent Assay (ELISA)

For protein isolation, the right lobes of the lungs were frozen in liquid nitrogen and kept at -80°C until analysis. Lung tissue was homogenized in a lysis buffer (PBS 1x, Triton X 0.01%, 1x Roche protease inhibitor cocktail, Roche Diagnostics, Mannheim, Germany) using TissueLyser. The total amount of biomarkers was quantified according to the manufacturer's protocol and normalized to the total content of protein which was quantified by Bradford's reagent (Sigma-Aldrich, St. Louis, MO, USA). Protein levels of interleukin (IL)-6, IL-1beta and keratinocyte chemoattractant (KC) were quantified in lung homogenate with ELISA kits, in accordance with the manufacturer's instructions (Peprotech, Cranbury, NJ, USA).

Statistical analysis

Different variables were compared using one-way analysis of variance (ANOVA), followed by the Tukey post hoc test. For in vivo analysis, we conducted Student *t* tests with *P* values adjusted for multiple comparisons ($n = 3$, $\alpha^* = 0.0167$, α^* Bonferroni-adjusted test). We used the Kolmogorov–Smirnov test with Lilliefors' correction and Levene's median test to assess the normality and equality of variance, respectively, for all the analysis of variance residuals, wherein all *P* values were ≥ 0.17 . Parametric data are expressed as means (standard deviation). All tests were conducted using GraphPad Prism version 9.1.1. (La Jolla, CA, USA). *P* values of < 0.05 were considered significant. A Venn diagram was created in the R environment with the Venn diagram package.

Results

Characterization of hUCMSC-EVs

We evaluated the physicochemical properties of hUCMSC-EVs obtained at different harvesting times (24, 48, and 72 h) by TEM, NTA, and nanoflow cytometry. In all samples, TEM analysis revealed the presence of hUCMSC-EVs with typical cup-like morphology and average size < 200 nm (Fig. 1A). Nanoparticle size distribution curves showed particles of 191.2 ± 6.6 , 170.3 ± 10.0 ,

and 168.0 ± 9.9 nm after 24, 48, and 72 h, respectively (Fig. 1B, C). The nanoparticle concentrations increased progressively from $2.63 \pm 0.25 \times 10^9$ and $4.52 \pm 0.48 \times 10^9$ particles/mL at 24 and 48 h ($P < 0.001$ versus 24 h), respectively, to $5.31 \pm 0.40 \times 10^9$ particles/mL at 72 h ($P < 0.0001$ versus 24 h) (Fig. 1D). The purity of the hUCMSC-EV preparations, measured as the ratio between the EVs and the protein concentrations, also progressively increased with time ($7.2 \pm 1.0 \times 10^9$, $14 \pm 2.9 \times 10^9$, and $26 \pm 12.0 \times 10^9$ particles/ μ g at 24, 48, and 72 h, respectively) (Fig. 1E). The rate of production of hUCMSC-EVs showed no significant changes between the timepoints ($1.2 \pm 0.17 \times 10^3$, $2.1 \pm 0.45 \times 10^3$, and $2.5 \pm 0.11 \times 10^3$ particles/cell at 24, 48, and 72 h, respectively) (Fig. 1F). The cells showed high viability ($86 \pm 3\%$) 72 h after the addition of the EV collection medium, suggesting a minor impact on cell viability.

Nanoflow cytometry analysis was used to provide a quantitative measure of hUCMSC-EV markers (Fig. S1). Analysis of the hUCMSC-EV sub-population between 100 and 500 nm showed the presence of the tetraspanins CD63 (13.01, 28.6, and 21.1% at 24, 48, and 72 h, respectively); CD81 (21.7, 40.4, and 32.8% at 24, 48, and 72 h, respectively); and CD90 (26.7, 47.3, and 44.0% at 24, 48, and 72 h, respectively).

Protein content of hUCMSCs and hUCMSC-EVs

Samples of hUCMSC-EVs typically consist of a heterogeneous mixture of small EVs and non-vesicular components [30]. We utilized LC-MS/MS to determine the protein composition of hUCMSC-EVs obtained at different harvesting times and compared these with their source cells (hUCMSCs). A total of 1,745 proteins were identified in the proteomic analysis of the source hUCMSCs, and 718 proteins were detected in hUCMSC-EVs according to UniProt accessions. The proteins quantified in hUCMSCs were compared to those in hUCMSC-EVs, and the results revealed that 470 proteins were shared between the source cells and their EVs, while 248 were exclusively detected in the hUCMSC-EV samples (Fig. 2A).

The proteins common to the hUCMSC and hUCMSC-EV samples, and those detected exclusively in hUCMSC-EVs were evaluated by GO analysis and summarized by BPs and cellular components. Cellular localization of the proteins shared by hUCMSCs and hUCMSC-EVs showed significant enrichment of 8 cellular compartments, including the cytoplasm, extracellular region, endoplasmic reticulum, endosome, lysosome, vacuole, nucleus, and ribosomes (Fig. 2B). The top 10 BPs associated with the higher number of proteins commonly found in hUCMSCs and hUCMSC-EVs included cell adhesion, protein stabilization, positive regulation of gene expression, and actin cytoskeleton organization (Fig. 2C). The GO analysis conducted against proteins present exclusively in hUCMSC-EV samples showed enriched terms related to the extracellular space, extracellular exosome, cytosol, extracellular matrix structural constituents, and protein binding (Fig. S2).

The proteome of hUCMSC-EV samples included proteins classified as: (1) transmembrane or GPI-anchored proteins associated with the plasma membrane and/or endosomes (i.e. CD63, CD81, CD82, GNAI2, ITGA, ITGB, LAMP1, LAMP2, SDC4, NT5E, HLA-A, CD9, CD90, and CD44); (2) cytosolic proteins recovered in EVs (i.e. ALIX, ANXA*, HSPA8, HSP90AB1, SDCBP, ACTB, and GAPDH); (3) major components of non-EV co-isolated structures (i.e. APOA1, APOA2, and APOB); (4) transmembrane, lipid-bound, and soluble proteins associated with intracellular compartments other than plasma membrane/endosomes (i.e. HIST1H2BC, HIST1H3A, HIST1H4A, HSPA5, HSP90B1, ACTN1, LMNA, and KRT18); and (5) secreted proteins recovered with EVs (i.e. TGFBI, TGFB2, PDGFC, FN1, and COL*) [7].

Evaluation of the protein abundance and PPI network analysis

The preliminary quantitative analysis of the protein content revealed that 65% of the proteins in the hUCMSC-EVs were compatible with the hUCMSC proteome (Fig. 3A). Comparing the hUCMSC-EV samples from the different harvest timepoints, the assays demonstrated an overlap of 415 proteins (58%), and less than 15% of proteins appeared exclusively at one timepoint,

implying a high degree of similarity between the samples (Fig. 3A). To gain further insight into the putative differences between the proteomic profile of hUCMSC-EVs, we investigated the abundance of proteins based on LFQ data according to specific conditions. The expression–abundance curve showed the proteins that have LFQ values greater than zero for at least one condition in each assay. The top 20 gene symbols of loaded proteins were selected for further analysis (Fig. 3B). To investigate the potential functions conducted by top-loaded proteins, the main BPs were evaluated using DAVID (<https://david.ncifcrf.gov/>). The most significant BP terms in common between the three groups (24, 48, and 72 h) comprised the following: response to mechanical stimulus, collagen fibril organization, extracellular matrix organization, wound healing, angiogenesis, and skin morphogenesis (Fig. 3C). The unique BP terms for assay were highlighted, and hUCMSC-EVs harvested at 24 h showed enriched proteins relating to the integrin-mediated signaling pathway, complement activation, and acute-phase response (Fig. S3), while the 72 h samples enriched processes associated with cell-matrix adhesion, regulation of NF- κ B signaling, and response to cytokines (Fig. S3).

The top-loaded proteins described were compared with proteins contained in EVs according to the Vesiclepedia public database (<http://microvesicles.org/>). According to the GO analysis, these proteins are involved in processes, such as angiogenesis, immune response, response to mechanical stimulus, wound healing, cell differentiation, and response to cytokine cell-matrix adhesion. To evaluate the interactions between the top-loaded proteins in hUCMSC-EV assays, PPI network analysis was conducted using STRING (Fig. S3). GO indicates several BPs associated with the selected proteins. In this analysis, proteins involved in cell differentiation, angiogenesis, and regulation of inflammatory response were highlighted. Furthermore, the top five proteins with the highest degree of interaction were investigated in all networks (Fig. 4A–C). The results indicated FN1, ACTB, COL1A1, HSP90AA1, EEF1A1, PSMA3, PSMA7, and ITGB1 as hubs, suggesting that these molecules play a central role in direct (physical), and indirect

(functional) associations among the detected proteins. Functional analysis of the proteins contained in the PPI network using STRING demonstrated that the selected hubs were mainly related to the following processes: immune effector, transport, localization, stress response, cellular activation, and response to stimulus (Fig. 4D).

Differential expression analysis

Differential expression analysis was conducted with hUCMSC-EV proteins from each harvesting time to identify enriched proteins. A volcano plot exhibited higher variability of differential proteins to indicate contrasts: 24 versus 48 h and 24 versus 72 h (fold change > 1.0 and P value < 0.05) (Fig. 5A). Heatmap analysis comparing the proteins at 24 and 48 h revealed two main clusters, and the proteins in cluster 1 were related to the innate immune response, positive regulation of B cell activation, phagocytosis, and positive regulation of receptor-mediated endocytosis (Fig. 5B). Cluster 2 comprised proteins involved in cellular response to hypoxia, negative regulation of cell population proliferation, negative regulation of mesenchymal cell proliferation, actin cytoskeleton organization, and actin filament network formation according to the UniProt database (<https://www.uniprot.org/>).

The comparison of proteins between 24 and 72 h showed that unique protein-coding gene clusters at 24 h were mainly involved in complement activation, particularly the classic pathway, as well as innate immune response, and the positive regulation of B cell activation (Fig. 5 C). These results showed that differential proteins had reduced variability at 48 h compared with those at 72 h, owing to the small rate of differentially expressed proteins among the assays; a complementary proteomics analysis was conducted on a pool of samples collected at different cultivation times. Fifteen of the top 20 most abundant proteins in the pool were also present in the 24-, 48-, and 72 h assays. In addition, these proteins were involved in skin morphogenesis, cellular response to amino acid stimulus, collagen fibril organization, and response to mechanical stimulus (Fig. S4).

In vivo biodistribution and toxicity analyses

Considering the high degree of similarity between the hUCMSC-EV samples collected at different timepoints, we used pooled hUCMSC-EVs for in vivo biodistribution and safety analyses. For the biodistribution analysis, DiR-labeled hUCMSC-EVs were intravenously administered to mice through the tail vein, followed by ex vivo analysis of different organs (brain, heart, lungs, liver, spleen, and kidneys) after 1 and 24 h (Fig. 6A). We observed a stronger fluorescent signal in the liver compared with that of the control after 1 h of IV administration (Fig. 6E, H). After 24 h, hUCMSC-EVs accumulated in the liver and spleen (Fig. 6E, F, I), showing a non-statistically significant tendency to accumulate in the lungs (Fig. 6C). We did not detect significant fluorescent signals exceeding the control levels in the other evaluated organs (brain, heart, and kidneys; Fig. 6A, D, G).

After the biodistribution evaluation, we investigated safety after single- and repeated-dose administrations (Fig. S5A). The body weight of the animals was measured to evaluate the general toxicity of hUCMSC-EVs and it did not vary among the groups ($P > 0.05$ for both groups; Fig. S5 B–E). The average counts of red blood cells, white blood cells, and platelets were also analyzed. At all timepoints, the mice injected with hUCMSC-EVs, either in a single or multiple doses, showed no significant hematologic changes compared with those in the control group ($P > 0.05$; Fig. S5 F, G). The effect of hUCMSC-EVs on liver and kidney function was evaluated by detecting the levels of AST, ALT, BUN, and Cr in the serum of mice. As presented in Tables S1 and S2, no significant differences were observed between the hUCMSC-EV and the control groups ($P > 0.05$). Histopathologic examination did not reveal any significant abnormalities or treatment-related changes in the analyzed heart, kidneys, lungs, spleen, liver, and brain tissues (data not shown).

To assess possible changes in the cellular composition of the spleen related to the immunogenicity, and immunotoxicity we evaluated the frequency of immune cells by flow

cytometry (Fig. 7). Flow cytometry analysis of immune sub-populations of the spleen showed no differences in the percentages of macrophages (CD45+CD11b+/F4-80+), B lymphocytes (CD45+/CD19+), and T lymphocytes (CD45+/CD3+) after 14 days, 3 and 6 weeks (Fig. 7B and C).

Acute lung injury

To further investigate the potential therapeutic effects of hUCMSC-EVs, we utilized a mouse model of LPS-induced ALI. The intratracheal administration of LPS resulted in alveolar collapse, alveolar inflammation as well as alveolar thickening in the LPS group compared with the control group. The cumulative diffuse alveolar damage (DAD) score was higher in the LPS group than in the control group ($P < 0.05$) (Fig. 8C). The administration of hUCMSC-EVs significantly reduced DAD score and histological changes compared with those treated with saline (Fig. 8 B, C). Levels of IL-1b, IL-6 and KC were higher in the LPS group compared with the control group ($P < 0.05$) and the treatment with hUCMSC-EVs significantly decreased the levels of all cytokines in lung tissue (Fig. 8D).

Discussion

EVs have garnered considerable attention as a mechanism of intercellular communication, and as candidates for therapeutic development as cell-free therapies [31]. In this study, we investigated the potential of hUCMSCs as a source of therapeutic EVs and provided an in-depth evaluation of the influence of culture and harvest conditions on the final product characteristics, including physical parameters and proteomic profile.

Compared with other tissue sources of MSCs, hUCMSCs have many advantages, such as the high availability of cord tissue, the high proliferative profile of cells, and their history of successful clinical translation, indicating safety and potentially beneficial effects [32-34]. In example, the safety and potential efficacy of hUCMSCs have been extensively studied in patients with severe Coronavirus disease-19 (COVID-19) in previous studies, including our own work [22,

34, 35]. The same hUCMSCs utilized as the source of EVs in here have been previously utilized to treat a patient with advanced critical COVID-19, showing significant immunomodulatory effects [22]. Switching from the therapeutic use of MSCs to their EVs could lead to a superior safety profile and provide several advantages in terms of logistics.

A major requirement in the field of therapeutic EVs is the optimization of large-scale manufacturing conditions, sustaining with high productivity and lot-to-lot consistency [36]. Repeated CM harvesting protocols are highly desirable to enhance the yield of EVs manufactured, but their implementation depend on the assessment of possible variability in the characteristics of the purified EVs in different timepoints. The harvest points studied here are within the range reported in the literature, usually comprising different intervals ranging from 12 h to 7 days [37]. We demonstrated a consistent production of hUCMSC-EVs for 72 h, with a progressive increase in productivity. Similar results regarding the EV productivity have recently been reported by others using different cell sources [38]. Regardless of the harvesting timepoints, the data indicate that hUCMSC-EVs were successfully isolated from hUCMSCs and met the minimum criteria to be classified as EVs [8, 39, 40]. Despite the remarkable similarity between the timepoints, proteomic data of hUCMSC-EVs revealed a small set of differentially expressed proteins at 24 h compared with that at 48 h and 72 h. The biological relevance and possible influence of these small differences on the safety, and therapeutic profile were not evaluated as the samples were not evaluated, as pooled samples were utilized in the in vivo studies, as recommended by the EVOLVE guidelines [41].

The analysis of proteomic data in hUCMSC-EVs indicated the presence of proteins involved in multiple cellular pathways relevant to health and disease, such as angiogenesis, immune response, response to mechanical stimulus, wound healing, cell differentiation, and response to cytokine cell-matrix adhesion. The proteomic analysis identified proteins that have previously been enriched in both small EVs (e.g., CD9, CD81, CD63, annexins, ALIX, and aldolase A) and the

non-vesicular fractions (GAPDH, PKM, HSP90, EEF2, PGK1, and clathrin) [30]. Although a significant overlap of protein content has been reported in small EVs and non-vesicle fractions, the results suggest that our samples included a mixture of small EVs and non-vesicle components, which is expected for the protocols of isolation and purification used herein. Furthermore, a mixture of exosomes and small microvesicles (CD81+/CD63+/CD9+, and annexin A1+) can be expected based on the analysis of protein content [30]. The nanoflow analysis presented here supports the frequency of classic exosomes estimated in approximately 20–30% of the EVs in the preparations. Quantitatively monitoring the frequency of exosome marker expression in each batch, rather than qualitative measurements, may be important to ensure the lot-to-lot consistency [30, 41].

Despite the increasing interest and the developments in the field of therapeutic EVs, only few studies have evaluated the biodistribution of EVs *in vivo* [42]. To evaluate the biodistribution of our product, we used a lipophilic dye - a method that allowed us to stain EVs while not altering the characteristics of the source cell (e.g. by genetic modification), and potentially, the characteristics of the final product, but that has been extensively criticized due to artifacts caused by dye aggregation, non-specific binding, and persistence [43]. Using this method, our results were consistent with the accumulation of EVs in the liver, spleen, and lungs, which is consistent with previous observations by others [44]. The identification of EVs in other organs and tissues has also been reported in protocols using higher doses, which could be related to the sensitivity of the detection methods [45]. EVs injected intravenously have been reported to be cleared by the reticuloendothelial system and may influence the local or systemic processes of injury and inflammation [46]. Whether this mechanism of clearance by innate immune cells could be a part of the mechanisms of immune regulation promoted by MSC-EVs still requires further investigation. Future studies using different methods for tagging EVs will be needed to address the

limitations of the lipid dye method and to study the interactions of MSC-EVs and cells of the reticuloendothelial system.

Our preclinical toxicology analysis that hUCMSC-EVs are safe after either a single systemic IV dose or even after 3- and 6 weeks-long repeated systemic administrations. This result is consistent with previous reports for EVs derived from MSCs, including a study wherein the repeated administration of hUCMSC-EVs showed no signs of immunogenicity [27]. Previous studies evaluating the toxicity of EVs from different sources corroborate our data, demonstrating their safety after IV administration in a single dose or in repeated administrations, even at extremely high doses, such as 2×10^{12} EVs/200 μ L/mouse, with no reports of acute or subacute toxicities in immunocompetent mice [47-49]. Intravenous administration of small extracellular vesicles isolated from hUCMSCs did not induce adverse reactions, such as hyperthermia, hemolysis, anaphylactic responses, or renal or hepatic dysfunction [50]. This underscores a potentially enhanced safety profile of MSC-derived EVs compared to their source cells, whose maximum tolerated dose has been established due to their pro-thrombotic activity at high concentrations. [51]. In contrast, EVs derived from other cell sources, such as tumor cells, are lethal at the same doses utilized herein, which highlights the importance of preclinical investigation of safety for different EV sources. For instance, a recent study showed that, when EVs derived from breast cancer cells were intravenously injected into immunocompetent BALB/c mice at doses of 50 or 100 μ g, they resulted in a high lethality rate, with no animals surviving beyond 24 hours post-injection. Therefore, the safety profile may vary depending on the type of source cell and the dosage of EVs administered [52].

Immune toxicity may occur with biological medicines and must therefore be evaluated as part of the preclinical toxicity assessment of EV products, especially considering that EVs target immune cells as part of their mechanism of action [53, 54]. Our data show that no significant differences were observed between the groups for any of the tested immune cell populations,

indicating that treatment with hUCMSC-EVs did not alter the composition of the immune cells in the spleen. Our results are in accordance with a previous study that demonstrated neither toxicity nor induction of an immune response in immunocompetent mice after repeated administrations of HEK293-derived EVs [55]. Our data, however, does not exclude the possibility of increased cytokine production or product-targeting immunoglobulins, which were not evaluated.

Finally, we studied the potential application of hUCMSC-EVs to treat ARDS, a severe pulmonary inflammatory disease, which has limited treatment options and presents with high morbidity and mortality among patients [56]. In this investigation, our results from histological studies and the production of pro-inflammatory cytokines and chemokines demonstrated that hUCMSC-EVs can reduce the LPS induced ALI in mice. Our data showed that hUCMSC-EVs can decrease amounts of the cumulative diffuse alveolar damage and the levels of IL1 beta, IL-6, and KC. In line with these observations, previous research has shown that systemic administration of either MSCs from bone marrow or their EVs lowers levels of TNF- α , IL-6, KC, VEGF, and TGF- β in ARDS models [28].

Conclusion

Our results demonstrate the feasibility of manufacturing hUCMSC-EVs under cGMP standards, maintaining consistent characteristics and safety profiles suitable for the future clinical development of cell-free therapies. Furthermore, hUCMSC-EVs were shown to reduce lung damage in mice with LPS-induced ALI by decreasing the levels of proinflammatory cytokines, which reinforces their potential to treat ARDS.

Abbreviations

ALT	Alanine aminotransferase
ANOVA	Analysis of variance
AST	Aspartate aminotransferase

ARDS	Acute respiratory distress syndrome
BP	Biological process
BUN	Blood urea nitrogen
cGMP	Current good manufacturing practice
Cr	Creatinine
CTRL	Control group
DAD	Diffuse alveolar damage
DAVID	Database for Annotation, Visualization, and Integrated Discovery
DEP	Differential enrichment analysis of proteomics
DiR	1,1-Dioctadecyl-3,3,3,3-tetramethylindotricarbocyanine iodide
EVs	Extracellular vesicles
GAPDH	Glyceraldehyde-3-phosphate dehydrogenase
GO	Gene Ontology
hUCMSC-EVs	Human umbilical cord MSC-derived EVs
i.v.	intravenous
i.p.	intraperitoneal
KC	keratinocyte chemoattractant
LC-MS/MS	Liquid chromatography-tandem mass spectrometry
LFQ	Label-free quantification
LPS	Escherichia coli lipopolysaccharide
MCH	Mean corpuscular hemoglobin
MCHC	Mean corpuscular hemoglobin concentration
MCV	Mean corpuscular volume
MSC	Mesenchymal stromal cell
NTA	Nanoparticle tracking analysis

PBS	Phosphate-buffered saline
PKM	Pyruvate kinase
PPI	Protein–protein interaction
RBC	Red blood cell
SDS	sodium dodecyl sulfate
TEM	Transmission electron microscopy

Declarations

Ethics approval and consent to participate

This study was approved by the Committee for the Use and Care of Animals in Research (CEUA) of the Animal Science of the Instituto Gonçalo Moniz (Fiocruz Bahia) under protocol number CEUA ID 021-2021. The production and characterization of hUCMSC-EVs from donor tissue was approved by the National Committee for Ethics in Research (CONEP, CAAE: 30724020.3.1001.0008). All participants gave written informed consent to participate.

Consent for publication

Not applicable.

Availability of data and materials

Data are available via ProteomeXchange with identifier PXD038850.

Competing interests

The authors declare that they have no competing interests.

Funding

This paper was funded by the Brazilian Council for Scientific and Technological Development (CNPq), the Rio de Janeiro State Research Foundation (FAPERJ), the Department of Science and Technology (DECIT)/Brazilian Ministry of Health, the Coordination for the Improvement of Higher Education Personnel (CAPES), National Institute of Science and Technology for

Regenerative Medicine, D'OR Institute Research & Education, and Maria Emilia Foundation. Funding organizations played no role in the design or conduct of the study, data interpretation, or writing of the article. Patricia R.M. Rocco (Research Productivity, PQ1A), Bruno Solano de Freitas Souza, Clarissa Araújo Gurgel Rocha (Research Productivity, PQ2) and Camila Indiani de Oliveira (Research Productivity, PQ1C) are supported by CNPq.

Authors' contributions

ZSMCF designed the study, performed *in vivo* experiments, analyses, and wrote the manuscript. GVR performed the bioinformatic analyses. KNS, BDP, and ECL performed cell cultures and EV purification, flow cytometry, and protein analyses. JDS performed the *in vivo* experiment in the ARDS model. JLSS and DLZ performed the mass spectrometry experiments. CPF performed the electron microscopy analyses. RBD and CAGR performed histologic processing and analyses. CIO performed spleen immunophenotyping analyses. LDM, LNMR, and EP performed the NTA analyses. PRMR and BSFS designed the study, provided funding, as well as wrote and reviewed the manuscript. All authors read and approved the final manuscript.

Acknowledgments

The authors would like to thank Ms. Roquelina Assis for technical support.

References

1. Margiana, R., et al., *Clinical application of mesenchymal stem cell in regenerative medicine: a narrative review*. Stem Cell Res Ther, 2022. **13**(1): p. 366.
2. da Silva, K.N., et al., *Is there a place for mesenchymal stromal cell-based therapies in the therapeutic armamentarium against COVID-19?* Stem Cell Res Ther, 2021. **12**(1): p. 425.
3. Dong, B., et al., *Exosomes from human umbilical cord mesenchymal stem cells attenuate the inflammation of severe steroid-resistant asthma by reshaping macrophage polarization*. Stem Cell Res Ther, 2021. **12**(1): p. 204.
4. Thomi, G., et al., *Exosomes derived from umbilical cord mesenchymal stem cells reduce microglia-mediated neuroinflammation in perinatal brain injury*. Stem Cell Res Ther, 2019. **10**(1): p. 105.
5. Welsh, J.A., et al., *Minimal information for studies of extracellular vesicles (MISEV2023): From basic to advanced approaches*. J Extracell Vesicles, 2024. **13**(2): p. e12404.
6. Jafarina, M., et al., *Mesenchymal Stem Cell-Derived Extracellular Vesicles: A Novel Cell-Free Therapy*. Immunol Invest, 2020. **49**(7): p. 758-780.

7. Dabrowska, S., et al., *Immunomodulatory and Regenerative Effects of Mesenchymal Stem Cells and Extracellular Vesicles: Therapeutic Outlook for Inflammatory and Degenerative Diseases*. Front Immunol, 2020. **11**: p. 591065.
8. Théry, C., et al., *Minimal information for studies of extracellular vesicles 2018 (MISEV2018): a position statement of the International Society for Extracellular Vesicles and update of the MISEV2014 guidelines*. J Extracell Vesicles, 2018. **7**(1): p. 1535750.
9. Maas, S.L.N., X.O. Breakefield, and A.M. Weaver, *Extracellular Vesicles: Unique Intercellular Delivery Vehicles*. Trends Cell Biol, 2017. **27**(3): p. 172-188.
10. van der Pol, E., et al., *Recent developments in the nomenclature, presence, isolation, detection and clinical impact of extracellular vesicles*. J Thromb Haemost, 2016. **14**(1): p. 48-56.
11. Agrahari, V., et al., *Extracellular Microvesicles as New Industrial Therapeutic Frontiers*. Trends Biotechnol, 2019. **37**(7): p. 707-729.
12. Yáñez-Mó, M., et al., *Biological properties of extracellular vesicles and their physiological functions*. J Extracell Vesicles, 2015. **4**: p. 27066.
13. Massa, M., et al., *Clinical Applications of Mesenchymal Stem/Stromal Cell Derived Extracellular Vesicles: Therapeutic Potential of an Acellular Product*. Diagnostics (Basel), 2020. **10**(12).
14. Salvadori, M., et al., *Dissecting the Pharmacodynamics and Pharmacokinetics of MSCs to Overcome Limitations in Their Clinical Translation*. Mol Ther Methods Clin Dev, 2019. **14**: p. 1-15.
15. Krampera, M. and K. Le Blanc, *Mesenchymal stromal cells: Putative microenvironmental modulators become cell therapy*. Cell Stem Cell, 2021. **28**(10): p. 1708-1725.
16. Vardaridou-Minasian, S. and M.J. Lorenowicz, *Mesenchymal stromal/stem cell-derived extracellular vesicles in tissue repair: challenges and opportunities*. Theranostics, 2020. **10**(13): p. 5979-5997.
17. Fernández-Santos, M.E., et al., *Optimization of Mesenchymal Stromal Cell (MSC) Manufacturing Processes for a Better Therapeutic Outcome*. Front Immunol, 2022. **13**: p. 918565.
18. Almeria, C., et al., *Heterogeneity of mesenchymal stem cell-derived extracellular vesicles is highly impacted by the tissue/cell source and culture conditions*. Cell Biosci, 2022. **12**(1): p. 51.
19. Curley, G.F., et al., *Cell-based Therapies for ARDS - Where Are We Now?* Am J Respir Crit Care Med, 2024.
20. Huang, Q., et al., *Signaling pathways and potential therapeutic targets in acute respiratory distress syndrome (ARDS)*. Respir Res, 2024. **25**(1): p. 30.
21. Bellani, G., T. Pham, and J.G. Laffey, *Missed or delayed diagnosis of ARDS: a common and serious problem*. Intensive Care Med, 2020. **46**(6): p. 1180-1183.
22. da Silva, K.N., et al., *Immunomodulatory and Anti-fibrotic Effects Following the Infusion of Umbilical Cord Mesenchymal Stromal Cells in a Critically Ill Patient With COVID-19 Presenting Lung Fibrosis: A Case Report*. Front Med (Lausanne), 2021. **8**: p. 767291.
23. Ribeiro, L.N.M., et al., *Use of nanoparticle concentration as a tool to understand the structural properties of colloids*. Sci Rep, 2018. **8**(1): p. 982.
24. Welsh, J.A., et al., *MIFlowCyt-EV: a framework for standardized reporting of extracellular vesicle flow cytometry experiments*. J Extracell Vesicles, 2020. **9**(1): p. 1713526.
25. Perez-Riverol, Y., et al., *The PRIDE database resources in 2022: a hub for mass spectrometry-based proteomics evidences*. Nucleic Acids Res, 2022. **50**(D1): p. D543-D552.
26. Golde, W.T., P. Gollobin, and L.L. Rodriguez, *A rapid, simple, and humane method for submandibular bleeding of mice using a lancet*. Lab Anim (NY), 2005. **34**(9): p. 39-43.
27. Rodrigues, S.C., et al., *Toxicological Profile of Umbilical Cord Blood-Derived Small Extracellular Vesicles*. Membranes (Basel), 2021. **11**(9).
28. Silva, J.D., et al., *Mesenchymal Stromal Cells Are More Effective Than Their Extracellular Vesicles at Reducing Lung Injury Regardless of Acute Respiratory Distress Syndrome Etiology*. Stem Cells Int, 2019. **2019**: p. 8262849.
29. Hsia, C.C., et al., *An official research policy statement of the American Thoracic Society/European Respiratory Society: standards for quantitative assessment of lung structure*. Am J Respir Crit Care Med, 2010. **181**(4): p. 394-418.
30. Jeppesen, D.K., et al., *Reassessment of Exosome Composition*. Cell, 2019. **177**(2): p. 428-445.e18.

31. Börger, V., et al., *International Society for Extracellular Vesicles and International Society for Cell and Gene Therapy statement on extracellular vesicles from mesenchymal stromal cells and other cells: considerations for potential therapeutic agents to suppress coronavirus disease-19*. *Cytotherapy*, 2020. **22**(9): p. 482-485.
32. Ahn, H., et al., *Treatment of acute ischemic stroke by minimally manipulated umbilical cord-derived mesenchymal stem cells transplantation: A case report*. *World J Stem Cells*, 2021. **13**(8): p. 1151-1159.
33. Xie, Q., et al., *What is the impact of human umbilical cord mesenchymal stem cell transplantation on clinical treatment?* *Stem Cell Res Ther*, 2020. **11**(1): p. 519.
34. Can, A., F.T. Celikkan, and O. Cinar, *Umbilical cord mesenchymal stromal cell transplantations: A systemic analysis of clinical trials*. *Cytotherapy*, 2017. **19**(12): p. 1351-1382.
35. Yang, C.W., et al., *Efficacy of umbilical cord mesenchymal stromal cells for COVID-19: A systematic review and meta-analysis*. *Front Immunol*, 2022. **13**: p. 923286.
36. Adlerz, K., et al., *Strategies for scalable manufacturing and translation of MSC-derived extracellular vesicles*. *Stem Cell Res*, 2020. **48**: p. 101978.
37. van Balkom, B.W.M., et al., *Proteomic Signature of Mesenchymal Stromal Cell-Derived Small Extracellular Vesicles*. *Proteomics*, 2019. **19**(1-2): p. e1800163.
38. Rayamajhi, S., et al., *Extracellular vesicles production and proteomic cargo varies with incubation time and temperature*. *Exp Cell Res*, 2023. **422**(2): p. 113454.
39. L Ramos, T., et al., *MSC surface markers (CD44, CD73, and CD90) can identify human MSC-derived extracellular vesicles by conventional flow cytometry*. *Cell Commun Signal*, 2016. **14**: p. 2.
40. Romanov, Y.A., et al., *Human Umbilical Cord Mesenchymal Stromal Cell-Derived Microvesicles Express Surface Markers Identical to the Phenotype of Parental Cells*. *Bull Exp Biol Med*, 2018. **166**(1): p. 124-129.
41. Silva, A.K.A., et al., *Development of extracellular vesicle-based medicinal products: A position paper of the group "Extracellular Vesicle translation to clinical perspectives - EVOLVE France"*. *Adv Drug Deliv Rev*, 2021. **179**: p. 114001.
42. Kang, M., et al., *Biodistribution of extracellular vesicles following administration into animals: A systematic review*. *J Extracell Vesicles*, 2021. **10**(8): p. e12085.
43. Chen, J., et al., *Impact of Pitx3 gene knockdown on glial cell line-derived neurotrophic factor transcriptional activity in dopaminergic neurons*. *Neural Regen Res*, 2017. **12**(8): p. 1347-1351.
44. Driedonks, T., et al., *Pharmacokinetics and biodistribution of extracellular vesicles administered intravenously and intranasally to*. *J Extracell Biol*, 2022. **1**(10).
45. Wiklander, O.P., et al., *Extracellular vesicle in vivo biodistribution is determined by cell source, route of administration and targeting*. *J Extracell Vesicles*, 2015. **4**: p. 26316.
46. Smyth, T., et al., *Biodistribution and delivery efficiency of unmodified tumor-derived exosomes*. *J Control Release*, 2015. **199**: p. 145-55.
47. Matsuda, A., et al., *Safety of bovine milk derived extracellular vesicles used for delivery of RNA therapeutics in zebrafish and mice*. *J Appl Toxicol*, 2020. **40**(5): p. 706-718.
48. Ha, D.H., et al., *Toxicological evaluation of exosomes derived from human adipose tissue-derived mesenchymal stem/stromal cells*. *Regul Toxicol Pharmacol*, 2020. **115**: p. 104686.
49. Ma, Y., et al., *Emerging Therapeutic Potential of Mesenchymal Stem Cell-Derived Extracellular Vesicles in Chronic Respiratory Diseases: An Overview of Recent Progress*. *Front Bioeng Biotechnol*, 2022. **10**: p. 845042.
50. Sun, L., et al., *Safety evaluation of exosomes derived from human umbilical cord mesenchymal stromal cell*. *Cytotherapy*, 2016. **18**(3): p. 413-22.
51. Giri, J. and J. Galipeau, *Mesenchymal stromal cell therapeutic potency is dependent upon viability, route of delivery, and immune match*. *Blood Adv*, 2020. **4**(9): p. 1987-1997.
52. Magoling, B.J.A., et al., *Membrane Protein Modification Modulates Big and Small Extracellular Vesicle Biodistribution and Tumorigenic Potential in Breast Cancers In Vivo*. *Adv Mater*, 2023. **35**(13): p. e2208966.
53. Brennan, F.R., et al., *Safety and immunotoxicity assessment of immunomodulatory monoclonal antibodies*. *MAbs*, 2010. **2**(3): p. 233-55.
54. McBlane, J.W., *Preclinical safety testing for cell-based products using animals*. *Biologicals*, 2015. **43**(5): p. 425-8.

55. Zhu, X., et al., *Comprehensive toxicity and immunogenicity studies reveal minimal effects in mice following sustained dosing of extracellular vesicles derived from HEK293T cells*. *J Extracell Vesicles*, 2017. **6**(1): p. 1324730.
56. Bellani, G., et al., *Epidemiology, Patterns of Care, and Mortality for Patients With Acute Respiratory Distress Syndrome in Intensive Care Units in 50 Countries*. *JAMA*, 2016. **315**(8): p. 788-800.

Figure Legends

Fig. 1 Characterization of hUCMSC-EVs purified from conditioned medium at different harvest timepoints. **A** Representative images of hUCMSC-EVs observed by transmission electron microscopy. **B** Representative curves of the size distribution and concentration of hUCMSC-EVs by nanoparticle tracking analysis (NTA). **C** Mean diameter of hUCMSC-EVs measured by NTA. **D** Concentration of hUCMSC-EVs measured by NTA. **E** Purity of EVs measured as the ratio between the nanoparticle and protein concentrations. **F** EVs productivity, measured by the ratio between total number of nanoparticles and the number of producer cells at each timepoint. * $P < 0.05$; ** $P < 0.01$; *** $P < 0.001$. hUCMSC-EVs, human umbilical cord mesenchymal stromal cell-derived extracellular vesicles.

Fig. 2 Protein identification and functional enrichment analysis of hUCMSCs and hUCMSC-EVs. **A** Venn diagram of the proteins detected in hUCMSCs against hUCMSC-EV samples and hUCMSC-EV proteins at different harvesting times (24, 48, and 72 h). **B** Gene Ontology (GO) cellular component of the shared proteins in hUCMSC and hUCMSC-EVs samples. The pie chart shows selected significantly enriched categories conducted with SubcellularRVis (<http://phenome.manchester.ac.uk/subcellular/>). **C** GO biological process of proteins in common in the hUCMSC and hUCMSC-EVs samples. Significantly enriched terms for biological process and cellular components were selected ($P < 0.05$). hUCMSC-EVs, human umbilical cord mesenchymal stromal cell-derived extracellular vesicles.

Fig. 3 Bioinformatics analysis of the top 20 most abundant proteins in hUCMSC-EVs samples. **A** Venn diagram showing the overlap between hUCMSC-EVs samples harvested at different timepoints. **B** Expression–abundance curve of hUCMSC-EVs samples based on label-free quantification. **C** Gene Ontology biological process terms in common displayed by the most abundant proteins found in the 24, 48, and 72h samples of hUCMSC-EVs. The bar represents the significance of terms for each condition ($-\log(P$ value). hUCMSC-EVs, human umbilical cord mesenchymal stromal cell-derived extracellular vesicles.

Fig. 4 Protein–protein interaction (PPI) network and hub analysis. **A–C** PPI network at 24 h (red), 48 h (blue), and 72 h (green). The top five hubs are highlighted in yellow. PPI networks were constructed with STRING and only interaction scores >0.7 were kept. **D** Gene Ontology biological processes terms enriched by protein hubs in the PPI network and identified by STRING (<https://string-db.org>). FDR, false discovery rate.

Fig. 5 Analysis of differential expression proteins (DEPs) performed for hUCMSC-EVs conditions. **A** Volcano diagram of DEPs in distinct hUCMSC-EVs harvesting times (24, 48, and 72 h) against pooled hUCMSC-EVs. **B** Heatmap of the protein levels of the DEPs. **C** Biological process enriched terms upregulated at 24 h in contrast with 48 and 72 h. FC, fold change; hUCMSC-EVs, human umbilical cord mesenchymal stromal cell-derived extracellular vesicles.

Fig. 6 Biodistribution study of hUCMSC-EVs *in vivo*. **A** Study design for evaluation of the biodistribution of DiR-labeled hUCMSC-EVs in mice after administration via the tail vein. **B–G** Quantification of the fluorescence intensity of different organs. Data are presented as means + standard deviation ($n = 3$). Asterisks indicate significant differences between the groups (** $P < 0.01$; *** $P < 0.001$; ANOVA followed by Tukey's test). **H, I** Representative *ex vivo* fluorescent images of DiR-labeled hUCMSC-EVs in liver and spleen at 1 h (H) and

24 h (I). DiR, 1,1-dioctadecyl-3,3,3,3-tetramethylindotricarbocyanine iodide; hUCMSC-EVs, human umbilical cord mesenchymal stromal cell-derived extracellular vesicles.

Fig. 7 Evaluation of immune cell populations in the spleen after single or repeated administration of EVs. **A** Gate strategy for the analysis of immune subpopulations in the spleen. **B** Percentage of macrophages, B and T lymphocytes in spleen samples 14 days after injection of hUCMSC-EVs. **C** Comparisons of macrophages, B and T lymphocytes after 3 and 6 weeks of Plasma-Lyte (CTRL) or injection of hUCMSC-EVs. hUCMSC-EVs, human umbilical cord mesenchymal stromal cell-derived extracellular vesicles.

Fig. 8 Therapeutic effects of hUCMSC-EVs in LPS-induced ALI model. **A** Schematic illustration of the ALI induction and EVs treatment in vivo. **B** Representative photomicrographs of lung stained with hematoxylin and eosin from the groups: CTRL, LPS and LPS-hUCMSC-EVs. Upper panels images were taken at 20x magnification and bars represent 50 μm . Lower panels images were taken at 40x magnification and bars represent 20 μm . **C** Diffuse alveolar damage (DAD) score. Data are presented as box plots of medians and interquartile ranges with 5-6 animals in each group. **D** ELISA was used to measure the protein expression levels of inflammatory cytokines, IL-1 β , IL-6 and keratinocyte chemoattractant (KC), after 24h hUCMSC-EVs administration. Asterisks indicate significant differences between the groups (*P < 0.05, **P < 0.01; ***P < 0.001; ANOVA followed by Tukey's test).

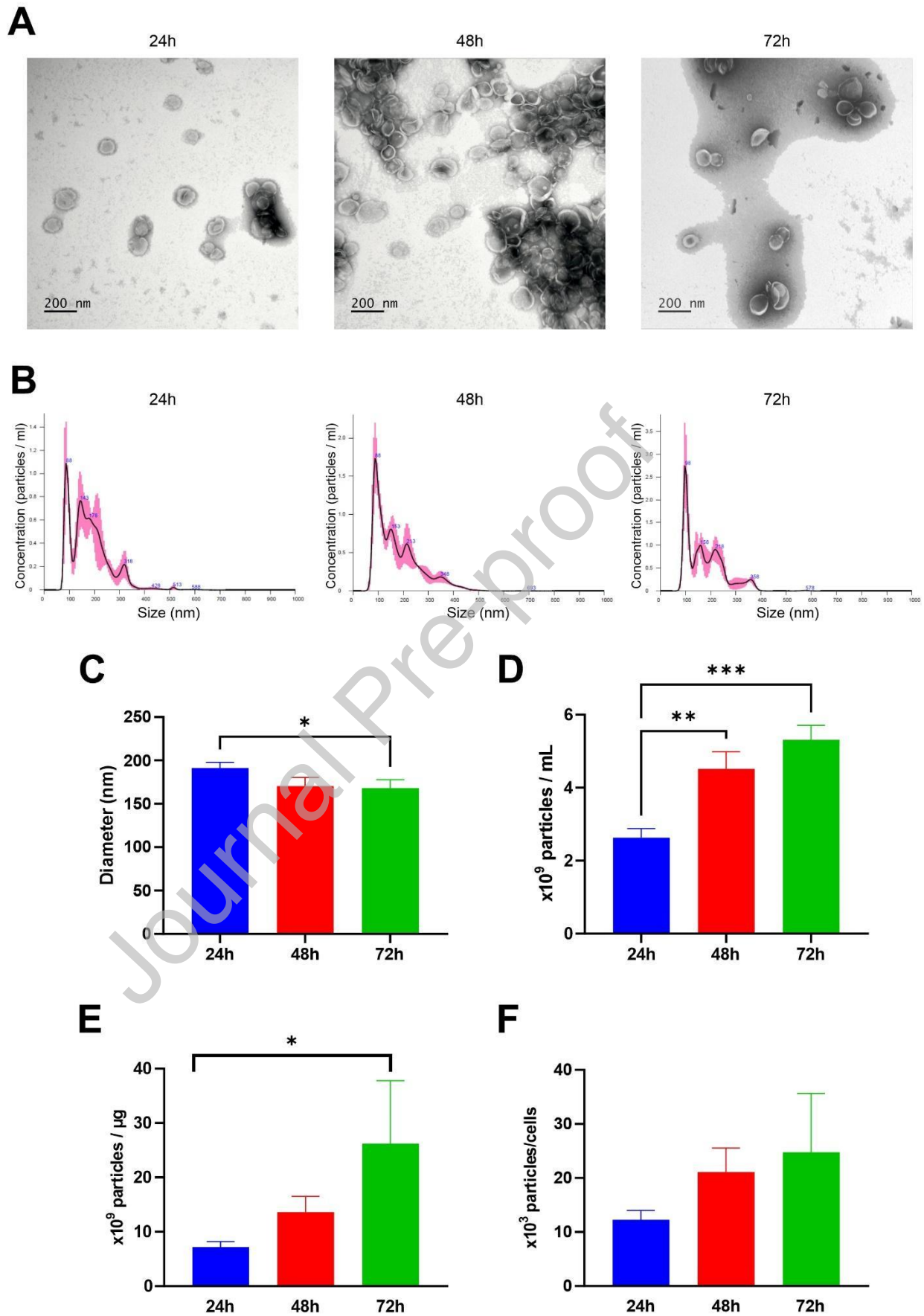


Figure 1.

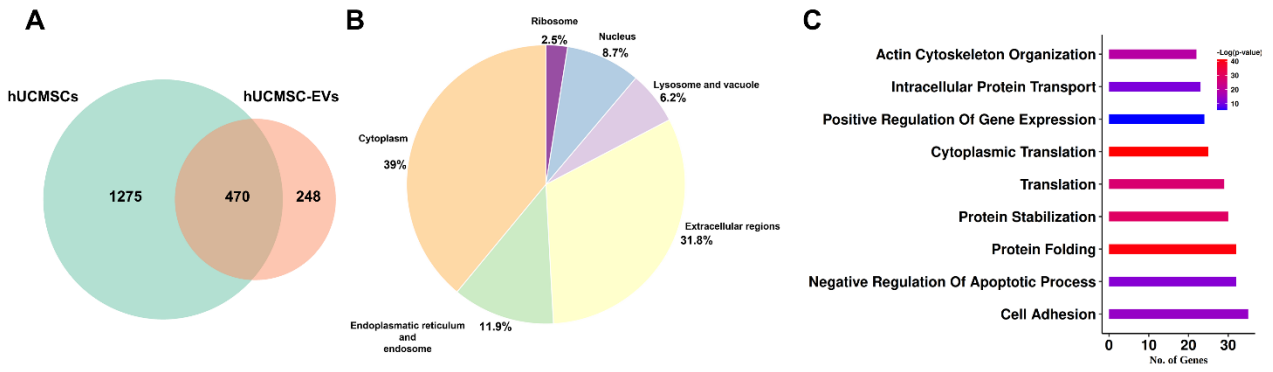


Figure 2.

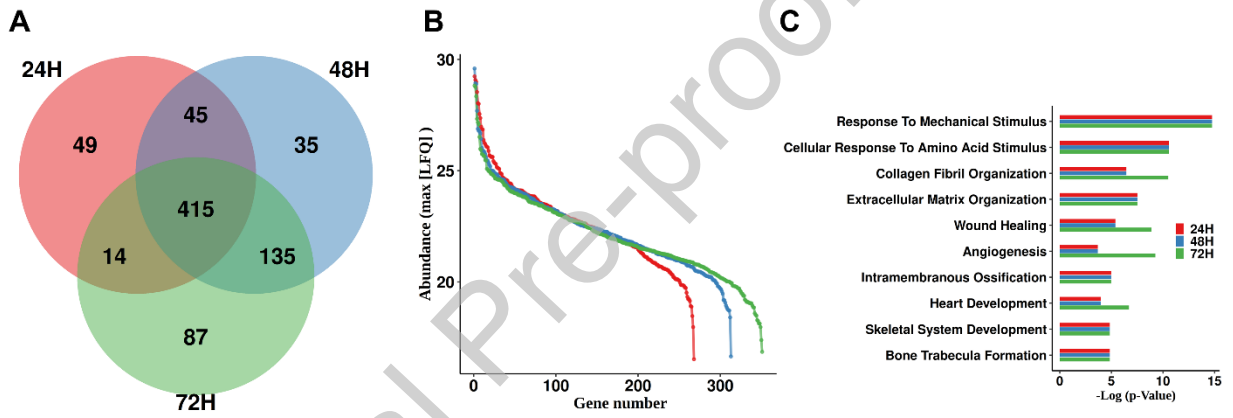


Figure 3

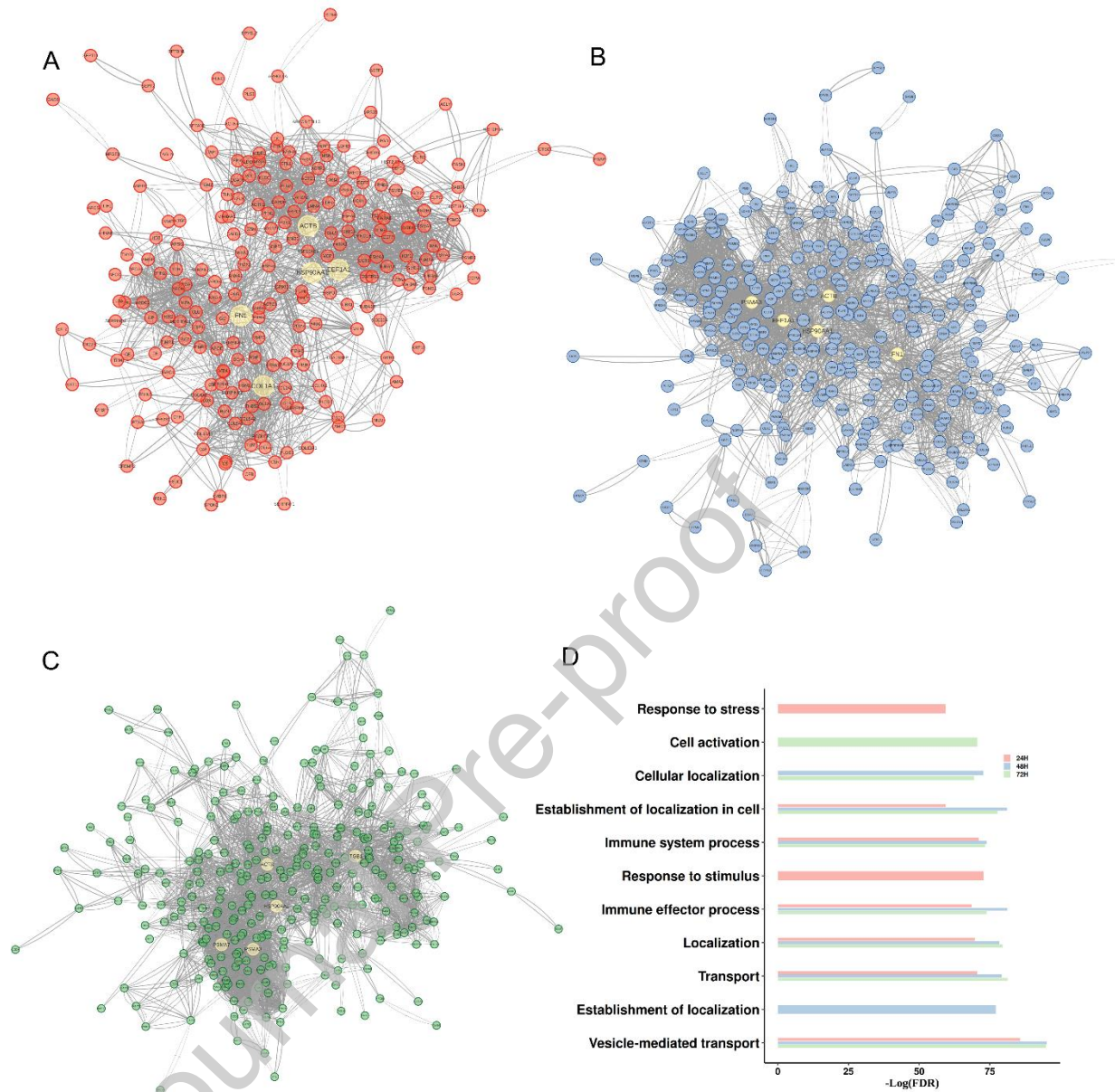


Figure 4.

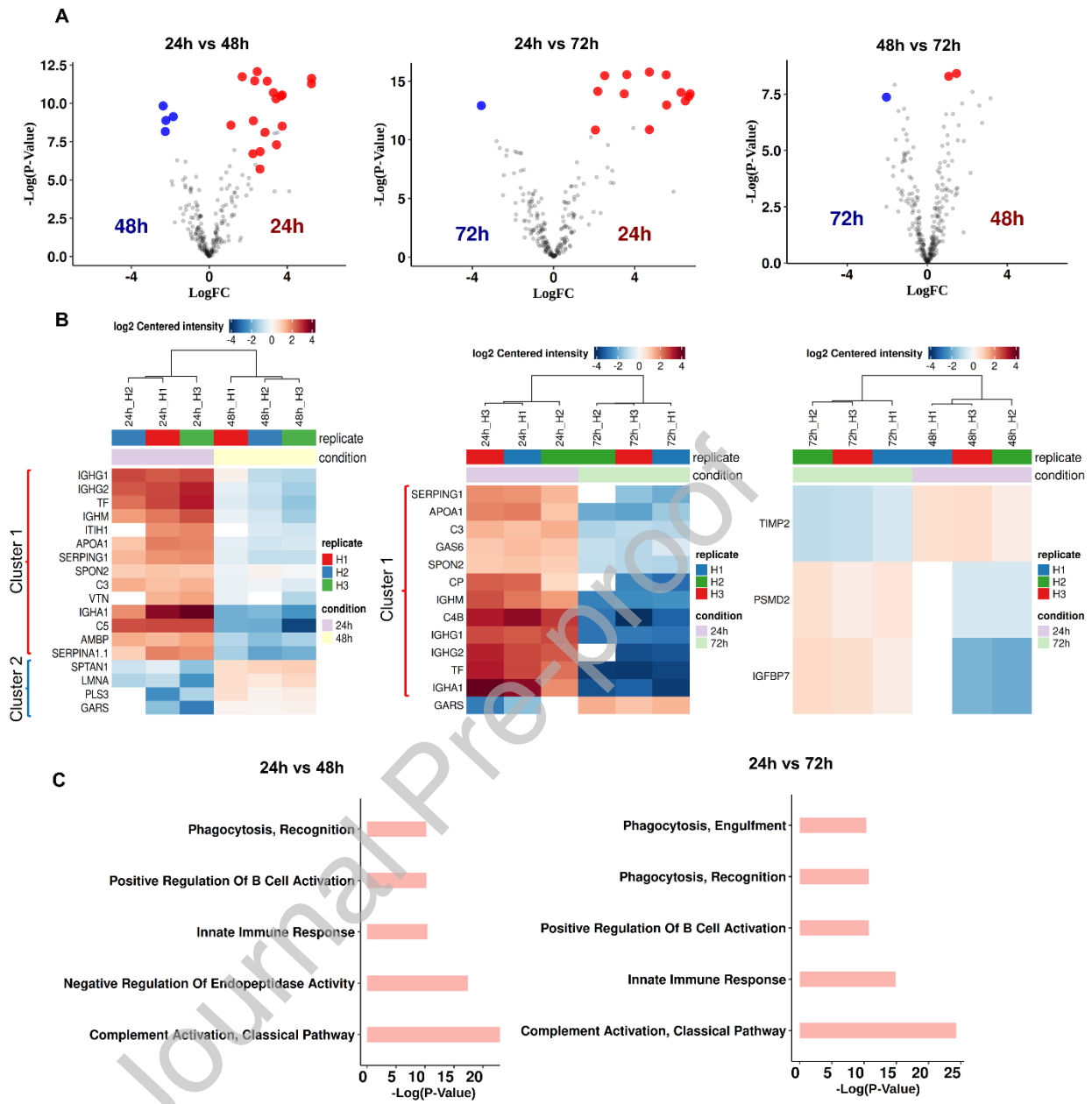


Figure 5.

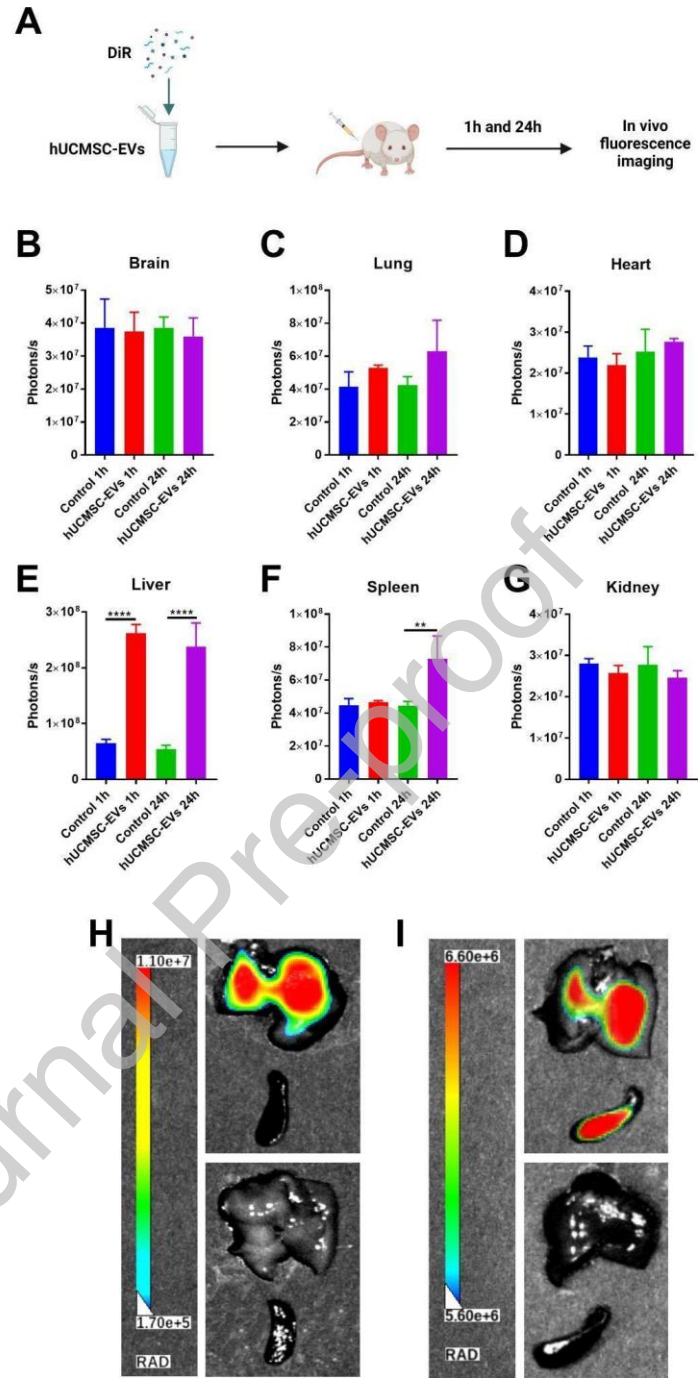


Figure 6.

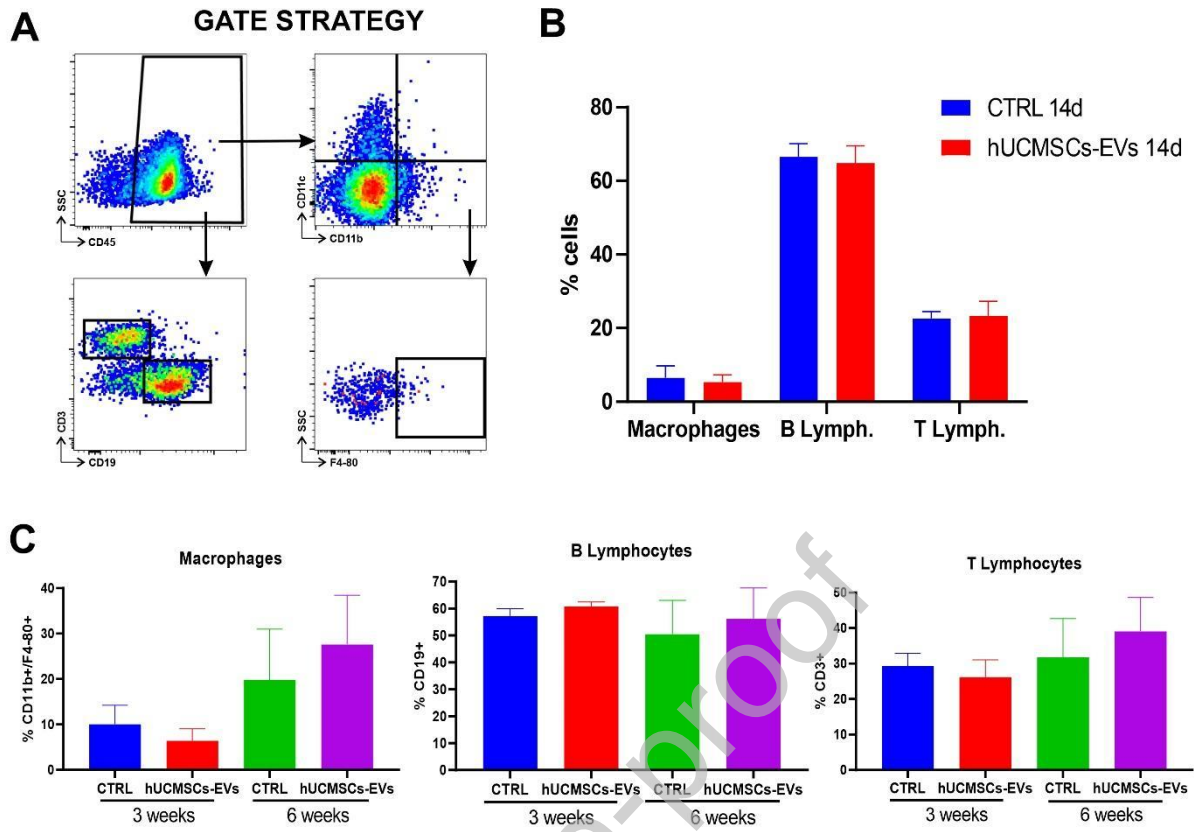


Figure 7

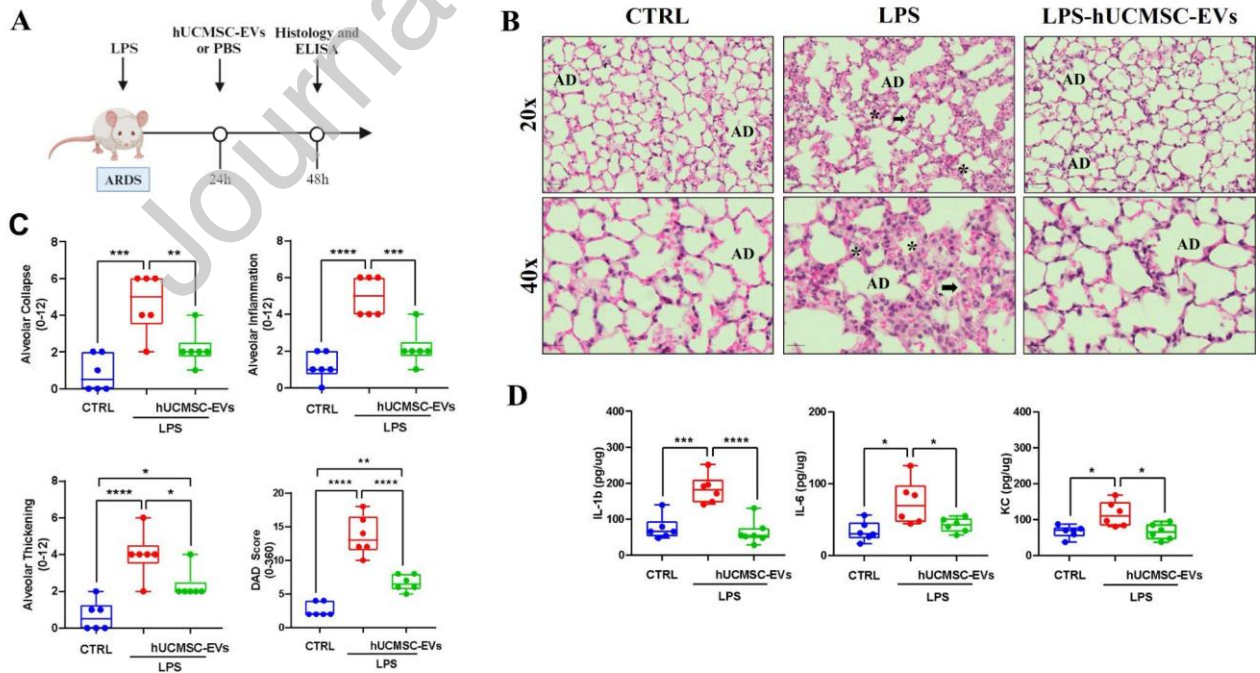


Figure 8